Journal of Solid State Chemistry 183 (2010) 1574–1581

Contents lists available at ScienceDirect

Journal of Solid State Chemistry

journal homepage: www.elsevier.com/locate/jssc

Phase relations and structural properties of the ternary narrow gap semiconductors $Zn_5Sb_4In_{2-\delta}$ ($\delta=0.15$) and $Zn_9Sb_6In_2$

Yang Wu [a], Andreas Tengå [b], Sven Lidin [b], Ulrich Häussermann [a,*]

[a] Department of Chemistry and Biochemistry, Arizona State University, Tempe, AZ 85287-1604, USA
[b] Inorganic Chemistry, Stockholm University, SE-10691 Stockholm, Sweden

ARTICLE INFO

Article history:
Received 12 February 2010
Received in revised form
27 April 2010
Accepted 2 May 2010
Available online 6 May 2010

Keywords:
Zinc antimonides
Narrow gap semiconductors
Superstructures

ABSTRACT

A systematic study of the Zn-rich corner of the ternary system Zn–Sb–In revealed the presence of two ternary compounds: stable $Zn_5Sb_4In_{2-\delta}$ ($\delta=0.15$) and metastable $Zn_9Sb_6In_2$ with closely related crystal structures. Their common motif is a tetragonal basic structure of 3^2434 nets formed by the Sb atoms. The nets are stacked in antiposition to yield layers of square antiprisms sharing edges plus intervening tetracapped tetrahedra (tetreadersterns). The majority of Zn atoms occupy peripheral tetrahedra of such tetraedersterns, which produces frameworks with a composition "ZnSb". These frameworks represent orthorhombic superstructures: $(2\times1\times1)$ for $Zn_5Sb_4In_{2-\delta}$ ($Z=4$) and $(2\times3\times1)$ for $Zn_9Sb_6In_2$ ($Z=8$) with respect to the tetragonal arrangement of Sb atoms. The In and remaining Zn atoms are distributed in the channels formed by the square antiprisms. Phase relations in the Zn–Sb–In system are complex. Crystals of metastable $Zn_9Sb_6In_2$ are regularly intergrown with various amounts of $Zn_5Sb_4In_{2-\delta}$. Additionally, a monoclinic variant to orthorhombic $Zn_9Sb_6In_2$ could be identified. $Zn_9Sb_6In_2$ decomposes exothermically into a mixture of $Zn_5Sb_4In_{2-\delta}$, Zn_4Sb_3 and elemental Zn at around 480 K. Both $Zn_5Sb_4In_{2-\delta}$ and $Zn_9Sb_6In_2$ are poor metals with resistivity values that are characteristic of heavily doped or degenerate semiconductors (0.2 – 3 m Ω cm at room temperature).

1. Introduction

Binary zinc and cadmium antimonides are capable of remarkable structural complexity which expresses itself in large, sometimes even giant unit cells and various forms of disorder [1–5]. Because of the low electronegativity difference between the divalent metal and antimony these structures represent weakly polar frameworks. Characteristically constituting atoms have coordination numbers larger than four while average valence electron concentrations are lower than four. Nevertheless, such frameworks realize a narrow band gap in the electronic structure at or close to the Fermi level [6,7]. The combination of structural complexity, weak polarity and a narrow band gap gives zinc and cadmium antimonides interesting thermoelectric properties which have been intensively investigated over the recent years [8].

The peculiar structural, bonding and electronic properties of zinc and cadmium antimonides are not easily maintained in ternary systems. For example, in conjunction with electropositive metals (alkali, alkaline earth and rare earth) typically Zn/Cd and Sb atoms form commonly polyanions in now rather polar Zintl phases [9]. Reactions with indium, however, provide an interesting possibility to modify the electron poor framework structures of zinc and cadmium antimonides while maintaining a weak polarity in the ternary compounds. Recently we reported on a ternary derivative of Cd_4Sb_3, $Cd_{13-x}In_ySb_{10}$, where trivalent indium appears to replace a considerable concentration of divalent cadmium [10]. This results in a framework structure which in contrast with Cd_4Sb_3 does not contain interstitial Cd atoms [5]. Similar attempts in the Zn–Sb–In system led to a different result. Contrary to the Cd–Sb–In system, indium does not produce a substitutional variant of a known zinc antimonide structure, but segregates into distinct crystallographic positions in new, ternary, crystal structures.

The exploration of the Zn–Sb–In system yielded hitherto two new phases, $Zn_5Sb_4In_{2-\delta}$ and $Zn_9In_6In_2$. $Zn_5Sb_4In_{2-\delta}$ represents a stable phase with highly interesting thermoelectric properties [11]. Herein we report on the synthesis and structure of metastable $Zn_9Sb_6In_2$ and its phase and structural relation to $Zn_5Sb_4In_{2-\delta}$.

2. Experimental section

2.1. Synthesis and phase characterization

All samples for the synthesis were prepared in a dry-argon filled glove box. Pure Zn (granules, 99.99%), Sb (powder, 99.5%)

* Corresponding author.
E-mail address: Ulrich.Haussermann@asu.edu (U. Häussermann).

0022-4596/$ - see front matter © 2010 Elsevier Inc. All rights reserved.
doi:10.1016/j.jssc.2010.05.001

and In (ingot, 99.99%) were purchased from Sigma–Aldrich. Powdered Sb was pressed into a pellet and all starting metals were loaded into silica tubes specially prepared for flux synthesis [12]. Total sample masses varied between 0.5 and 1 g. Specific sample compositions are compiled in Fig. 1 and discussed later.

After flame sealing under vacuum ($<10^{-4}$ mbar) ampoules were placed into a well insulated stainless-steel container. Reactions were carried out in a box furnace with a programmable temperature controller. First, the temperature was raised to 923 K and kept for 24 h to homogenize the metal mixture. Subsequently the temperature was lowered to 598–748 K at rates between 2 and 5 K/h and the reaction mixture held at this temperature for 48 h. The actual holding temperature depended on the composition of the reaction mixture and was chosen high enough to maintain flux conditions. This procedure resulted in mm-sized specimens of agglomerated crystals which were separated from the liquid excess metal mixture by centrifugation. The intermetallic products are air and moisture stable.

For phase analysis powder X-ray diffraction patterns were collected on a Bruker D8 Advance diffractometer (Cu$K\alpha$ radiation). Thermal behavior was investigated by differential thermal analysis (Shimadzu DTA-50). Samples constituting of crystal pieces were sealed in stainless steel containers in the glove box. The experiments were preformed under a flow of dry Ar in a temperature interval from 300 to 830 K and with a temperature increase rate of 5 K/min.

2.2. Crystal structure characterization

Crystals suitable for single crystal X-ray diffraction were obtained by crushing specimens obtained by flux synthesis. Intensity data collection was performed at room temperature (295 K) on an Oxford Diffraction Xcalibur 3 CCD diffractometer with monochromatic Mo$K\alpha$ radiation (λ=0.71073 Å) operated at 50 kV and 40 mA. The sample-to-detector distance was 50 mm. Oxford Diffraction's CrysAlis software was employed for data reduction [13].

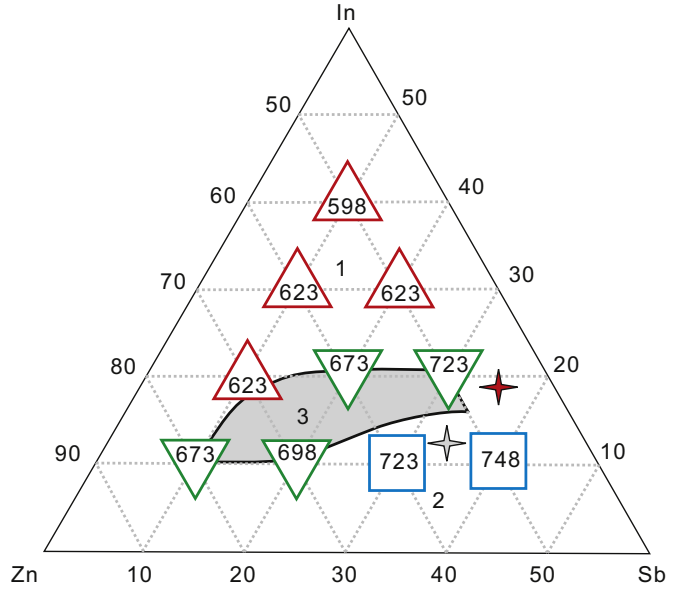

Fig. 1. Synthesis diagram for $Zn_5Sb_4In_{2-\delta}$ and $Zn_9Sb_6In_2$. Colored symbols demark investigated compositional areas with temperatures inscribed that are necessary for maintaining flux conditions. Product regions: **1**—(red, upward triangles): $Zn_5Sb_4In_{2-\delta}$ with traces of InSb; **2**—(blue, squares): Zn_4Sb_3; **3**—green (downward triangles): product mixture of $Zn_5Sb_4In_{2-\delta}$ and Zn_4Sb_3 upon radiant cooling; **3**—gray area: $Zn_9Sb_6In_2$ upon quenching. Compositions on axes are in at%. The red and gray stars mark the compound compositions for $Zn_5Sb_4In_{2-\delta}$ and $Zn_9Sb_6In_2$, respectively. (For interpretation of the references to color in this figure legend, the reader is referred to the web version of this article.)

The diffraction patterns of both the previously described room-temperature form of $Zn_5Sb_4In_{2-\delta}$ [11] and the here presented $Zn_9Sb_6In_2$, can be interpreted as orthorhombic superstructures of a tetragonal, *I*-centered, basis lattice with $a_{tet}\approx 8.7$ Å and $c_{tet}\approx 7.15$ Å. The room temperature structure of $Zn_5Sb_4In_{2-\delta}$ has space group symmetry *Pbcn* with $a\approx c_{tet}$, $b\approx 2\times a_{tet}$, $c\approx a_{tet}$. For $Zn_9Sb_6In_2$ a_{tet} appears doubled and b_{tet} trebled. The symmetry of the basic structure is *I*4/*mcm*. In orthorhombic setting this yields the full set of symmetry operations (I (2,2$_1$)/(*c*,*b*) (2,2$_1$)/(*c*,*a*) (2,2$_1$)/(*m*,*n*)). Now, doubling or trebling an axis can never convert a glide operation to a reflection (while the reverse is possible), and since there are no systematic absences for the *h k* 0, *h* 0 *l* or 0 *k l* planes, the only possible reflection operation in the cell is the mirror plane perpendicular to *c*. In orthorhombic symmetry, the allowed combinations of two-fold axes and reflections are limited to 2/*m* 2/*m* 2/*m*, *mm*2, *m*2*m*, 2 *mm* and 222, and hence, the lone reflection perpendicular to *c* is disallowed as well. The orthorhombic space group must therefore be generated by a combination of 2-fold rotations and 2$_1$ screws. Inspection of the axial reflections reveals systematic absences compatible with $P2_12_12_1$ and that was the space group used to solve the structure. To phase the reflections, charge flipping [14], as implemented in the program Superflip [15] was used. This yielded a set of atomic positions that quickly refined to an acceptable agreement between F^2 data and model if twinning was properly modelled. For this the program JANA2000 was employed [16]. The final model treats all atomic positions with anisotropic thermal displacement parameters. In $Zn_5Sb_4In_{2-\delta}$, we detected a substantial occupational deficiency for the In positions [11], and the structural model for $Zn_9Sb_6In_2$ was tested for In deficiency as well. Allowing occupational deficiency of the In positions did not result in any change of the overall composition, although two In positions became over-occupied and the other two under-occupied. The effect is slight, and the difference in fit between model and data is negligible. Consequently, the structure was treated as stoichiometric with all atomic positions fully occupied. Table 1 lists a summary of the refinement results of orthorhombic $Zn_9Sb_6In_2$ and a monoclinic variant, which is addressed later on. Details are supplied as supporting information, or can be obtained from the Fachinformationszentrum Karlsruhe, 76344 Eggenstein-Leopoldshafen, Germany (fax: +49 7247 808 666; E-mail: crysdata@fiz-karlsruhe.de) on quoting the depository numbers CSD-421504 (orthorhombic $Zn_9Sb_6In_2$) and CSD-421505 (monoclinic $Zn_9Sb_6In_2$).

2.3. Electrical resistivity measurements

The electrical resistivity of $Zn_9Sb_6In_2$ was measured on a Physical Property Measurement System (PPMS) from Quantum Design using a four-point probe in-line configuration. Needle-shaped crystals were selected from different synthesis batches and gently polished to remove any excess metal residual on the surface. Typical specimen dimensions were $0.5\times 0.5\times 5.0$ mm^3. Gold bonding wires (0.03 mm) were painted on the sample and electrodes on the resistivity puck using an air-drying silver paint (Demetron D200) for contacts. The puck was subsequently loaded into the PPMS chamber and then evacuated and sealed for the measurement. A constant current of 1 mA was applied and the resistance recorded from 10 to 350 and 350 to 10 K (one heating/cooling cycle) at a rate of 1 K/min.

Table 1
Selected crystallographic data for the orthorhombic and monoclinic form of $Zn_9Sb_6In_2$.

Crystal data	Orthorhombic	Monoclinic
Formula	$Zn_9Sb_6In_2$	$Zn_9Sb_6In_2$
Formula weight	1548.6	1548.6
Space group	$P2_12_12_1$	$P2_111$
a (Å)	7.142(2)	7.142
b (Å)	17.146(5)	17.146
c (Å)	25.719(7)	51.439
Beta (deg)		90
Z; V (Å^3)	8; 3149.4(15)	16; 6299
D_{calc} (g cm^{-3})	6.53	6.53
Temp (K)	293	293
λ (Mo$K\alpha$) (Å)	0.71069	0.71069
Absorption coeff. (mm^{-1})	26.347	26.347
F(000)	5391	10,784
ω_{min}–ω_{max} (deg)	2.38–28.37	4.43–26.89
Index ranges	$-9 \le h \le 9$, $-22 \le k \le 22$, $-34 \le l \le 34$	$-8 \le h \le 8$, $-18 \le k \le 21$, $-63 \le l \le 54$
Total reflns collected	21,287	25,164
Independent reflns	7183	17,525
Refinement method	Full-matrix least-squares on F^2	Full-matrix least-squares on F^2
Data/restraints/ params	7183/0/308	17,525/0/224
Final R indices $[I > 3\sigma(I)]$[a,b]	R_1=0.0408, wR_2=0.0837	R_1=0.1259, wR_2=0.1354
R indices (all data)[a,b]	R_1=0.1885, wR_2=0.1028	R_1=0.1611, wR_2=0.1393
Largest diff. peak and hole (e Å^{-3})	3.21, −3.11	7.40, −9.01
GOF on F^2	1.6	3.85

[a] $R_1 = ||F_o| - |F_c||/|F_o||$.
[b] $wR_2 = [w(F_o^2 - F_c^2)^2]/[w(F_o^2)^2]^{1/2}$.

3. Results and discussion

The Zn-rich corner of the ternary phase diagram was systematically investigated. Fig. 1 summarizes the applied reaction mixtures used and corresponding temperatures where flux conditions are maintained. (Note that synthesis temperatures increased with increasing Sb concentrations.) Additionally the products are indicated. With respect to reaction products one can discern three regions: (1) High In concentrations yield the ternary compound $Zn_5Sb_4In_{2-\delta}$. (2) High Sb concentrations (and accompanying higher temperatures) favor the formation of Zn_4Sb_3. (3) A mixture of $Zn_5Sb_4In_{2-\delta}$ and Zn_4Sb_3 is obtained in the intermediate region.

Importantly, attempts to synthesize $Zn_5Sb_4In_{2-\delta}$ from stoichiometric melts always produced a mixture of $Zn_5Sb_4In_{2-\delta}$, Zn_4Sb_3 and InSb, which indicates that the ternary compound melts incongruently. In contrast, flux synthesis with higher In (and Zn) concentrations (i.e. region (1)) yields $Zn_5Sb_4In_{2-\delta}$ virtually phase pure and in the form of mm-sized crystals. Depending on synthesis temperature and composition the product may contain small amounts of InSb. Fig. 2a shows representatively the powder pattern of the product from the synthesis mixture $Zn_{50}Sb_{20}In_{30}$ annealed at 623 K.

A second ternary compound, later established as $Zn_9Sb_6In_2$, was first recognized in a reaction mixture $Zn_{62.5}Sb_{25}In_{12.5}$

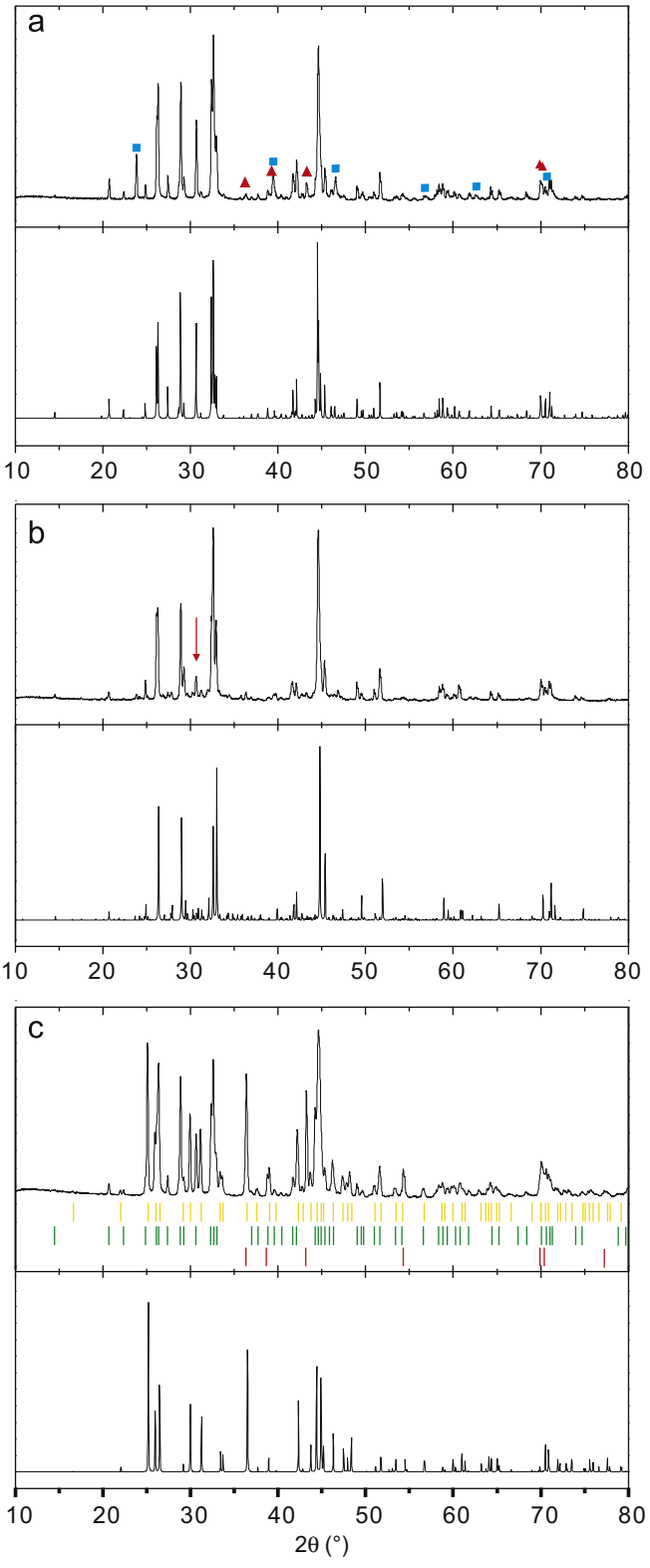

Fig. 2. (a) Powder XRD pattern (Cu$K\alpha$) for the product of sample $Zn_{50}Sb_{20}In_{30}$ (top). Square and triangle symbols mark reflections from the byproducts InSb and Zn, respectively. The calculated pattern for $Zn_5Sb_4In_{2-\delta}$ is shown below. (b) Powder XRD patterns for the product of sample $Zn_{60}Sb_{25}In_{15}$ (top). This product represents a macroscopic mixture of $Zn_9Sb_6In_2$ and a small amount of byproduct $Zn_5Sb_4In_{2-\delta}$. The arrow marks a reflection from $Zn_5Sb_4In_{2-\delta}$. Discrepancies between measured and calculated pattern around $2\theta = 33^\circ$ are also attributed to this byproduct. Additionally, crystals of $Zn_9Sb_6In_2$ contain various amounts of microscopically intergrown $Zn_5Sb_4In_{2-\delta}$. The calculated pattern for $Zn_9Sb_6In_2$ is shown below. (c) Powder XRD pattern of the product mixture obtained after annealing $Zn_9Sb_6In_2$ at 573 K (top). $Zn_9Sb_6In_2$ decomposes quantitatively into $Zn_5Sb_4In_{2-\delta}$, Zn_4Sb_3 and elemental Zn, indicated with yellow, green and red reflection markers, respectively. The calculated pattern below is for β-Zn_4Sb_3. (For interpretation of the references to color in this figure legend, the reader is referred to the web version of this article.)

annealed at 723 K, but could subsequently not be reproduced. This raised the suspicion that the compound may be metastable and decomposing if not quenched. In the routine way of finishing off reactions, crystalline products were left in the insulated stainless steel container after centrifugation to cool radiantly to room temperature (cf. Section 2). Indeed, when silica jackets were taken out of the steel container immediately after centrifugation and quenched in ice water the crystalline product corresponded reproducibly to $Zn_9Sb_6In_2$. Subsequently a larger number of reactions were repeated and finished off by quenching. This procedure yielded $Zn_9Sb_6In_2$, together with minor amounts of $Zn_5Sb_4In_{2-\delta}$, for the compositional region that previously afforded a product mixture of $Zn_5Sb_4In_{2-\delta}$ and Zn_4Sb_3 (i.e. region (2), Fig. 1). Fig. 2b shows representatively the powder pattern of the product from the synthesis mixture $Zn_{60}Sb_{25}In_{15}$ annealed at 698 K and subsequently quenched. The great similarity to the powder pattern of $Zn_5Sb_4In_{2-\delta}$ indicates a very close structural similarity.

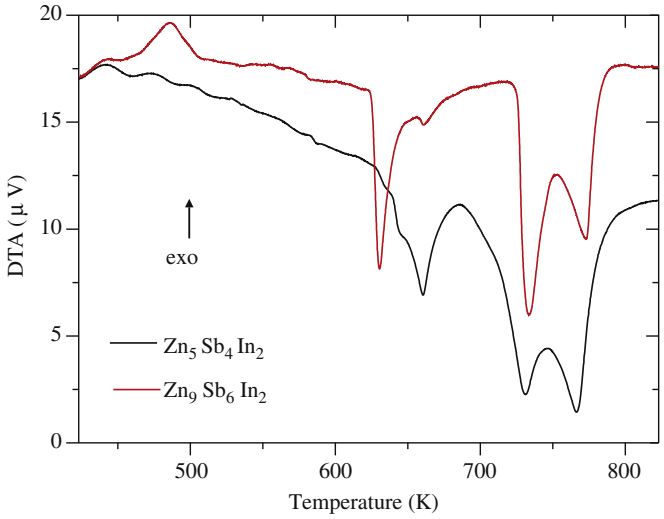

Fig. 3. DTA heating trace for $Zn_9Sb_9In_2$ (red line) and $Zn_5Sb_4In_{2-\delta}$ (black line). (For interpretation of the references to color in this figure legend, the reader is referred to the web version of this article.)

The metastable nature of $Zn_9Sb_6In_2$ was confirmed in DTA experiments (Fig. 3). The broad exothermic event in the trace for $Zn_9Sb_6In_2$ with a maximum around 485 K is attributed to its decomposition into the thermodynamically stable mixture. Powder X-ray diffraction analysis of a sample $Zn_9Sb_6In_2$ annealed at 573 K for 1 h identifies the constituents of this mixture as $Zn_5Sb_4In_{2-\delta}$, Zn_4Sb_3 and elemental Zn (Fig. 2c). Thermal events at higher temperatures (above 600 K) must be inherent to this mixture. $Zn_5Sb_4In_{2-\delta}$ undergoes several high temperature phase transitions above 573 K, which are not well investigated yet, and decomposes at a temperature between

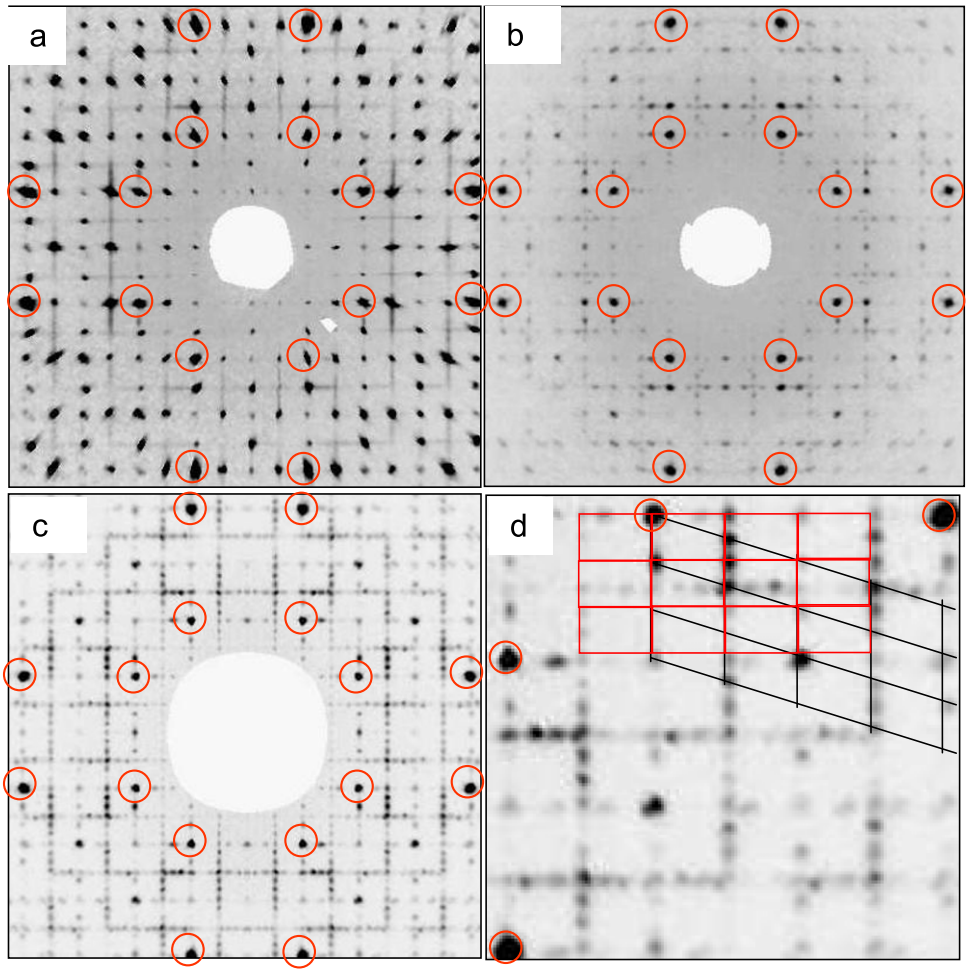

Fig. 4. Diffraction patterns corresponding to $h\,k\,1\,\ell$ of (a) orthorhombic $Zn_5Sb_4In_{2-\delta}$, (b) orthorhombic $Zn_9Sb_6In_2$ and (c) a monoclinic and orthorhombic two-phase crystal $Zn_9Sb_6In_2$. The reflections corresponding to the basic tetragonal lattice are highlighted. The diffraction pattern shown in (d) represents an enlargement of (c) where the reciprocal unit cells of orthorhombic and monoclinic $Zn_9Sb_6In_2$ have been highlighted.

750 and 800 K. Events in the trace for $Zn_9Sb_6In_2$ above 700 K resemble that for pure $Zn_5Sb_4In_{2-\delta}$.

Single crystal X-ray diffraction studies revealed further intricacies in the phase relation between $Zn_9Sb_6In_2$, $Zn_5Sb_4In_{2-\delta}$, and also Zn_4Sb_3. Structurally, $Zn_9Sb_6In_2$ turns out to be quite challenging. As for the previously reported $Zn_5Sb_4In_{2-\delta}$ there is a basic tetragonal pattern (Fig. 4a) arising from the Sb substructure ($I4/mcm$). In $Zn_5Sb_4In_{2-\delta}$ the systematic extinction associated with the I-centering is broken, and additionally both the a and b directions exhibit satellite reflections that indicate a doubling of the corresponding axes. There is however a conspicuous lack of reflections that double the tetragonal a and b axes simultaneously, and this led us to conclude that the doubling only applies to one direction, while the second set of satellites is generated by pseudomerohedral twinning. The space group symmetry of $Zn_5Sb_4In_{2-\delta}$ is $Pbcn$ with $a \approx 7.15$ Å (c_{tet}), $b \approx 17.15$ Å ($2 \times a_{tet}$) and $c \approx 8.7$ Å (a_{tet}).

The diffraction pattern of $Zn_9Sb_6In_2$ is more complex, and a cursory inspection indicates a tetragonal unit cell with a six-fold superstructure along the a and b directions (Fig. 4b). A very large number of reflections are however systematically absent, indicating twinning. With few exceptions the non-crystallographic absences are in agreement with a model where a_{tet} is doubled and b_{tet} is trebled. Pseudomerohedral twinning generates the rest of the reflections observed. The violations of this simple model are a weak set of reflections that double a_{tet} and b_{tet} simultaneously, and those reflections will be dealt with separately at a later stage. $Zn_9Sb_6In_2$ was assigned space group symmetry $P2_12_12_1$.

A large number of crystals were studied, and in many samples the fit between data and model was quite poor, but improved substantially when $Zn_5Sb_4In_{2-\delta}$ was introduced into the refinement as a second phase. It appears that substantial fractions of $Zn_5Sb_4In_{2-\delta}$ intergrow regularly with metastable $Zn_9Sb_6In_2$. The reverse situation is observed as well. However, the volume fractions of $Zn_9Sb_6In_2$ in crystals of thermodynamically stable $Zn_5Sb_4In_{2-\delta}$ are significantly smaller (up to 8%) [11].

One particular crystal showed a distinctly different diffraction pattern. The six-fold super-structuring is much more pronounced than in $Zn_9Sb_6In_2$ and interestingly, this effect is exhibited only in every second row of reflections (Fig. 4c). The obvious interpretation is a further doubling of the long axis in $Zn_9Sb_6In_2$ but this approach proved unsuccessful in providing a structural solution. After abandoning this first interpretation, it was realized that the diffraction pattern may be generated by a two-phase crystal, where one phase is orthorhombic $Zn_9Sb_6In_2$ and the other is a monoclinic variant that generates a new set of reflections along the long axis that neatly interdigitates the reflections from the former (Fig. 4d). The symmetry of this new monoclinic phase was assumed to be $P2_111$, and the structure was solved by charge flipping. It comes out as a simple variation of the orthorhombic form. The structure of the monoclinic form may be generated by a simple shift of a unit cell sized block of the orthorhombic phase by the vector $(0\frac{1}{2}\frac{1}{2})$. To facilitate the simultaneous treatment of the two structures, the shift vector $(0\frac{1}{2}\frac{1}{2})$ was employed as a centering vector in the monoclinic structure. This allows a description in a metrically orthorhombic cell, twice the size of the cell of the orthorhombic phase (doubling the long b-axis). Thus, both structures are described in a metrically orthorhombic cell measuring 7.14 Å × 17.14 Å × 51.44 Å. (The orthorhombic phase possesses a centering vector of $(0\frac{1}{2}\frac{1}{2})$ in this setting.) In addition to

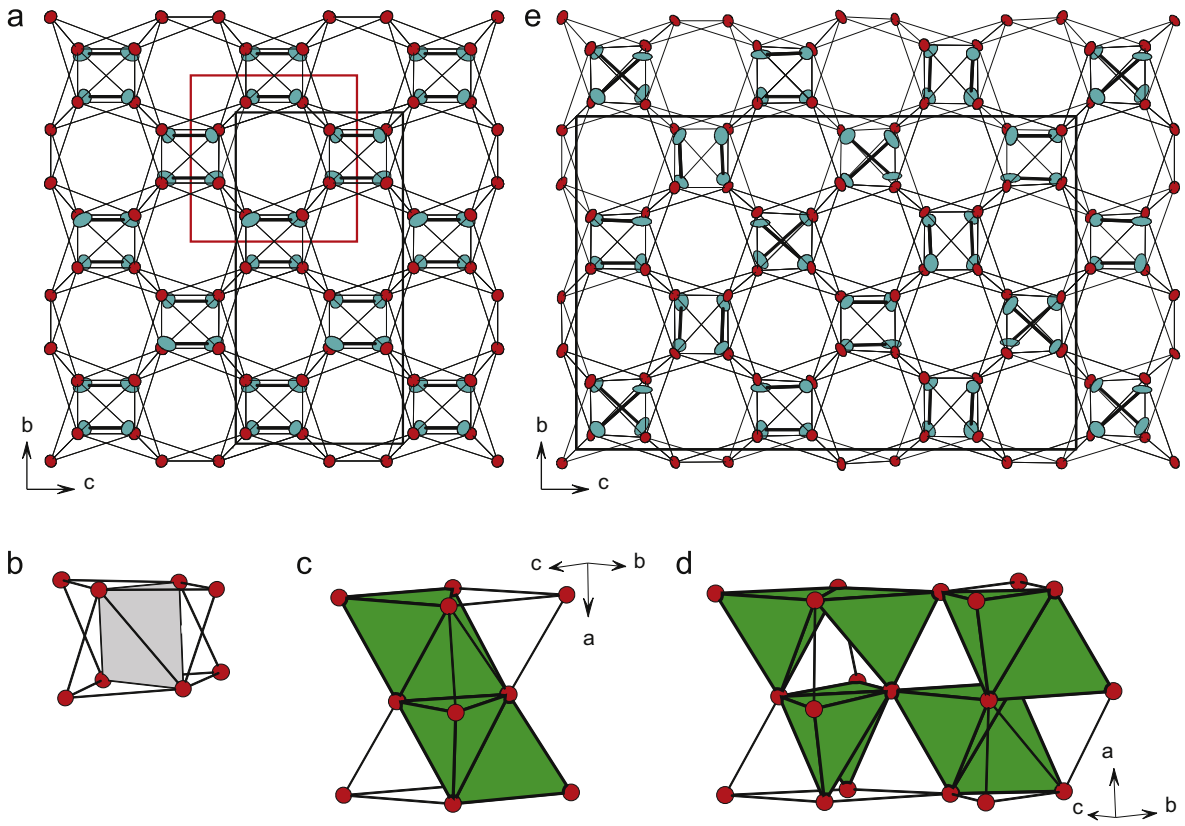

Fig. 5. (a) The framework "ZnSb" in $Zn_5Sb_4In_{2-\delta}$. Sb atoms (red) form 3^2434 nets (thin lines) stacked in antiposition orientation. Atom pairs Zn–Zn (cyan) are connected by black, thick, lines. The unit cell of the Sb atom arrangement is outlined in red, the one of the $Zn_5Sb_4In_{2-\delta}$ structure in black. (b) Tetracapped tetrahedron ("tetraederstern") formed by 8 Sb atoms. The central tetrahedron (empty) is marked in gray. (c) Arrangement of tetraedersterns in $Zn_5Sb_4In_{2-\delta}$ with half of the peripheral tetrahedra occupied by Zn atoms (marked in green). (d) Filling pattern of peripheral tetrahedra in $Zn_9Sb_6In_2$. (e) The framework "ZnSb" in $Zn_9Sb_6In_2$. Ellipsoids are drawn at a 90% probability. (For interpretation of the references to color in this figure legend, the reader is referred to the web version of this article.)

the biphasic nature of the crystal, both phases are twinned by pseudomerohedry because of the underlying tetragonal symmetry. The final agreement between model and data is modest (R_1 is ca. 12%, cf. Table 1), but considering the complexity of the sample this is not unexpected.

The most prominent satellite reflections of the monoclinic phase are those that simultaneously double the *a* and *b* axes of the basic tetragonal cell. It is interesting to note that these reflections are absent both in $Zn_5Sb_4In_{2-\delta}$ and in orthorhombic $Zn_9Sb_6In_2$. These are the unexplained weak reflections present in the diffraction pattern of $Zn_9Sb_6In_2$ referred to earlier. It would seem that metastable $Zn_9Sb_6In_2$ occurs in different structural variations depending on melt composition and the thermal history of sample preparation. The same holds for the intergrowth with $Zn_5Sb_4In_{2-\delta}$. Finally, it should be mentioned that we also identified crystals were $Zn_9Sb_6In_2$ appears to be epitaxially intergrown with the binary phase Zn_4Sb_3. This shows the complexity of phase relations in the compositional region (2), even nominal "single" crystals may consist of several phases.

In the following, we establish the crystal structure relationships between orthorhombic $Zn_5Sb_4In_{2-\delta}$ and $Zn_9Sb_6In_2$ (Figs. 5 and 6). The characteristic features of both structures are 3^2434 nets formed by the Sb atoms that are stacked in antiposition orientation (Fig. 5a). This arrangement is body centered tetragonal (the unit cell is indicated in Fig. 5a) and also yields rows of face-sharing square antiprisms that are connected in the tetragonal plane by sharing triangle edges. Such an arrangement of 3^2434 nets occurs in many intermetallic compounds; most prominent is probably the $CuAl_2$ type where nets are formed by Al atoms while Cu atoms center square antiprisms [17]. In addition to square antiprisms the Sb atom substructure generates also intervening tetracapped tetrahedra usually termed tetreadersterns (Fig. 5b) [17].

In $Zn_5Sb_4In_{2-\delta}$ and $Zn_9Sb_6In_2$ Zn atoms occupy two of the four peripheral tetrahedra in Sb_8 tetreadersterns. Since tetrahedra share edges, this results in rather short Zn−Zn distances (below or close to 3 Å). The distribution of Zn atoms (or "Zn pairs") is shown in Fig. 5c. In $Zn_5Sb_4In_{2-\delta}$, Zn atoms of a pair are always at different heights with respect to the stacking direction of 3^2434 nets and in the same orientation, which gives rise to a "parallel" pattern in the projection along the stacking direction (cf. Fig. 5a). In $Zn_9Sb_6In_2$ this distribution is more complex (Fig. 5d and e): 1/3 of the pairs are formed by Zn atoms at the same height, giving rise to a "cross" pattern, whereas 2/3 of the pairs are arranged in the "parallel" fashion, however, with alternating orientation (ratio 1:1). Note, that in our previous paper on $Zn_5Sb_4In_{2-\delta}$, where we preliminarily addressed $Zn_9Sb_6In_2$, we erroneously stated that the distribution of Zn atoms in tetrahedral interstices is the same in both structures [11]. It is, however, clearly different.

The filling patterns of Zn atoms in peripheral tetrahedra result in a symmetry lowering of the originally tetragonal arrangement of Sb_8 tetraedersterns to orthorhombic. The framework of Sb and Zn atoms in $Zn_5Sb_4In_{2-\delta}$ and $Zn_9Sb_6In_2$ represent $(2\times1\times1)$ and $(2\times3\times1)$ superstructures, respectively, with respect to the tetragonal basis structure of Sb atoms. It has a composition "ZnSb", with 16 and 48 formula units, respectively, in the unit cell. The frameworks "ZnSb" are highly unusual when considering the structures of $Zn_5Sb_4In_{2-\delta}$ and $Zn_9Sb_6In_2$ as derivatives of the $CuAl_2$ type. None of the ubiquitous structures based on antiposition stackings of 3^2434 nets and different fillings of square antiprisms and tetrahedra display this kind of distribution [17]. However, when focusing on shortest interatomic distances in the frameworks, Zn–Zn and Zn–Sb, structural fragments characteristic for binary zinc antimonides (ZnSb and Zn_4Sb_3) emerge.

The fraction of remaining atoms ("$ZnIn_2$"=$Zn_5Sb_4In_2$−"Zn_4Sb_4" and "Zn_3In_2"=$Zn_9Sb_6In_2$−"Zn_6Sb_6") is located in the

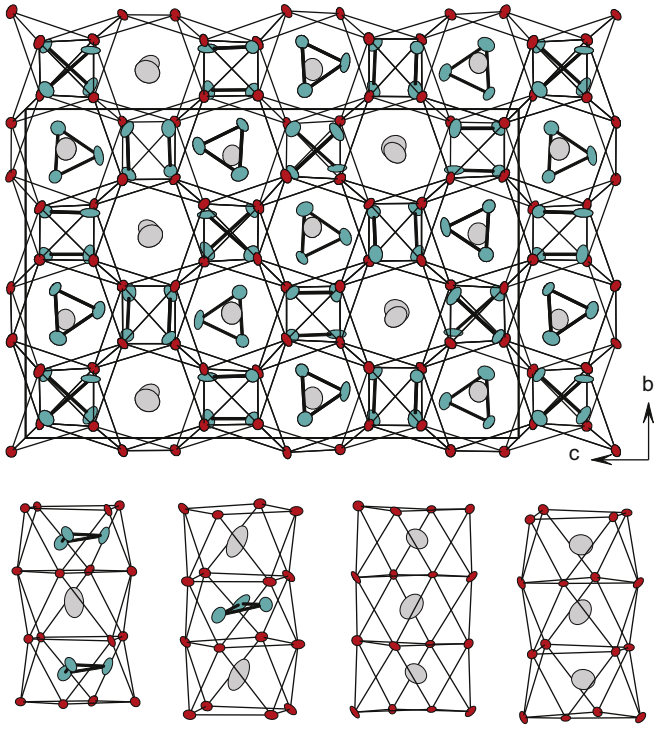

Fig. 6. (a) The total structure of $Zn_9Sb_6In_2$ projected along the stacking direction of 3^2434 net. Cyan, red and gray ellipsoids denote Zn, Sb and In atoms, respectively. Atom pairs Zn–Zn are connected by black, thick lines. (b) Filling of four symmetry independent tetragonal channels in $Zn_9Sb_6In_2$. Ellipsoids are drawn at a 90% probability. (For interpretation of the references to color in this figure legend, the reader is referred to the web version of this article.)

channels provided by the rows of square antiprisms in the "ZnSb" frameworks ([11] and Fig. 6a). For $Zn_5Sb_4In_{2-\delta}$ centers of square antiprisms are occupied alternately by pairs of Zn and In atoms, and single In atoms. The In positions in $Zn_5Sb_4In_{2-\delta}$ display some occupational deficiency (5–10%) which is indicated as δ in the compound formula. The value of δ is 0.15 and does not appear to be variable, suggesting that $Zn_5Sb_4In_{2-\delta}$ has no or only a very small homogeneity range. Instead of pairs Zn–In and single In atoms for $Zn_5Sb_4In_{2-\delta}$ triangles of Zn atoms (Zn_3) and In atoms in a ratio 1:2 occur for $Zn_9Sb_6In_2$ (Fig. 6a). Their arrangement within square antiprisms is shown in Fig. 6b. The Zn–Zn contacts within triangles correspond to the shortest interatomic distances in the structure of $Zn_9Sb_6In_2$ (2.5–2.6 Å). As aforementioned, in contrast with $Zn_5Sb_4In_{2-\delta}$ occupational deficiency of In atoms could not be detected for $Zn_9Sb_6In_2$. The structure of the monoclinic form of $Zn_9Sb_6In_2$ is shown in Fig. 7. It is simply generated by a shift of unit cell sized blocks of the orthorhombic structure by half of the translational period in the *b* direction (cf. Fig. 6a).

Previously it has been shown that $Zn_5Sb_4In_{2-\delta}$ has promising thermoelectric properties [11]. As a matter of fact, in the investigated temperature interval 10–350 K it is superior to state-of-the-art Zn_4Sb_3 as a thermoelectric material. Especially remarkable is the thermal conductivity of $Zn_5Sb_4In_{2-\delta}$: low magnitudes (around 1 W/m K) occur over the whole range of temperatures, and a peak at low temperatures characteristic for crystalline materials is absent [18,19]. This peculiar behavior has been attributed to the presence of intergrown domains of $Zn_9Sb_6In_2$ in $Zn_5Sb_4In_{2-\delta}$, turning this material to a phonon glass. Despite the inclusion of small fractions $Zn_9Sb_6In_2$, $Zn_5Sb_4In_{2-\delta}$ crystals and bulk samples can be considered as compositionally rather homogenous. Diffraction patterns and measured properties do not significantly vary for specimens from different samples.

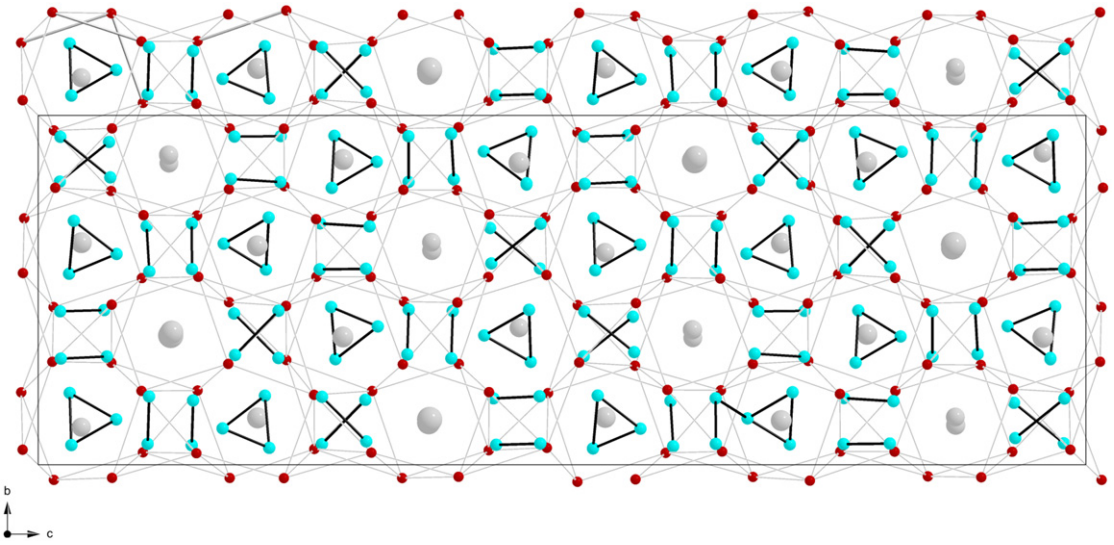

Fig. 7. Structure of monoclinic $Zn_9Sb_6In_2$ presented in an *A*-centered, metrically orthorhombic, unit cell. The color code of atoms is the same as in Fig. 6.

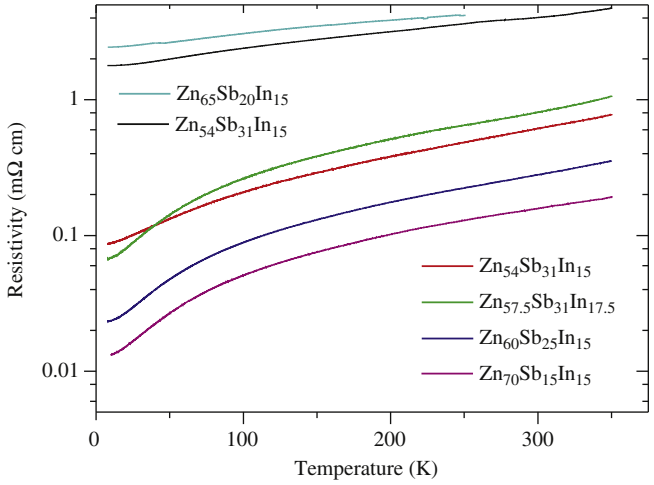

Fig. 8. Electrical resistivity of various specimens of $Zn_9Sb_6In_2$. The composition of their synthesis mixture is indicated in the plot.

This is not the case for $Zn_9Sb_6In_2$ where specimens contain variable amounts of intergrown $Zn_5Sb_4In_{2-\delta}$ (and possibly also Zn_4Sb_3). Additionally, $Zn_9Sb_6In_2$ can occur in different modifications with slightly different structures.

Indeed, electrical resistivity (ρ) measurements between 10 and 350 K on a large number of $Zn_9Sn_6In_2$ specimens showed a rather broad range of resistivity values (Fig. 8). The extremes differ by an order of magnitude. We do not find an apparent correlation of resistivity values and synthesis compositions used for producing the $Zn_9Sb_6In_2$ specimens. Generally, the temperature dependence of the resistivity is metal-like and magnitudes (m Ω cm range) are typical of a poor metal or heavily doped semiconductor. Specimens with high resistivity seem to show a weaker temperature dependence. As a matter of fact, the slope of $\rho(T)$ and also magnitudes of ρ up to temperatures around 220 K are very similar to $Zn_5Sb_4In_{2-\delta}$ [11]. After this temperature, however, $\rho(T)$ for $Zn_5Sb_4In_{2-\delta}$ changes into semiconductor-like [11]. It may be assumed that specimens displaying a high resistivity contain a large(r) fraction of intergrown $Zn_5Sb_4In_{2-\delta}$, and that $Zn_9Sb_6In_2$ has a lower intrinsic resistivity than $Zn_5Sb_4In_{2-\delta}$.

The average valence electron concentration of the ternary Zn–In–Sb frameworks is low, 3.27 for $Zn_5Sb_4In_{2-\delta}$ when considering an ideal situation with fully occupied In positions ($\delta=0$), and 3.18 for $Zn_9Sb_6In_2$. The electronic density of states (DOS) of both compounds has been recently calculated [7]. The DOS for idealized $Zn_5Sb_4In_2$ displays a narrow band gap with a size of 0.2 eV, and the Fermi level would be situated at this gap if the In positions were fully occupied. For more electron-poor $Zn_9Sb_6In_2$ a similar situation is obtained, however, the gap, where the Fermi level is located, appears just closed.

Although detailed features of the bonding interactions between In and the "ZnSb" framework in these ternary compounds are not yet clear, it is interesting to note that despite of the low values of electron concentration narrow band gaps at or close the Fermi level can still be realized. The electrical resistivity behavior of both materials is compatible with a stoichiometric $Zn_9Sb_6In_2$ where the Fermi level is at a closed band gap, and a non-stoichiometric $Zn_5Sb_4In_{2-\delta}$ possessing a proper band gap but having the Fermi level shifted slightly into the valence band through the In deficiency.

4. Conclusions

The exploration of the Zn-rich section of Zn–Sb–In system yielded two ternary intermetallic compounds, stable $Zn_5Sb_4In_{2-\delta}$ ($\delta=0.15$) and metastable $Zn_9Sb_6In_2$ with closely related crystal structures. Their common features are 3^2434 nets of Sb atoms that are stacked in antiposition orientation. Although this is a prominent structural motif of intermetallic compounds, the distribution of Zn and In atoms in the square antiprismatic and tetrahedral voids provided by the Sb atom arrangement is unique and results in novel structure types. The electronic structure of $Zn_5Sb_4In_{2-\delta}$ and $Zn_9Sb_6In_2$ resembles that of binary zinc antimonides in that a narrow band gap, or pronounced pseudogap, is realized at or close to the Fermi level. The electrical resistivity of both materials is typical of poor metals or degenerate semiconductors.

Acknowledgments

This work was supported by the Swedish Research Council (VR) and the National Science Foundation through Grants DMR-0638826, DMR-1007557and CHE-0742006. We are grateful to Dr. N. Newman, ASU, for supporting this research by generously making his PPMS available.

Appendix A. Supporting information available

Crystallographic data in CIF format for orthorhombic and monoclinic $Zn_9Sb_6In_2$. Tables of atomic position parameters and interatomic distances for orthorhombic $Zn_9Sb_6In_2$.

Appendix B. Supplementary material

Supplementary data associated with this article can be found in the online version at doi:10.1016/j.jssc.2010.05.001.

References

[1] G.J. Snyder, M. Christensen, E. Nishibori, T. Caillat, B.B. Iversen, Nat. Mater. 3 (2004) 458.
[2] J. Nylén, M. Andersson, S. Lidin, U. Häussermann, J. Am. Chem. Soc. 126 (2004) 16306.
[3] J. Nylén, S. Lidin, M. Andersson, B.B. Iversen, H.X. Liu, N. Newman, U. Häussermann, Chem. Mater. 19 (2007) 834.
[4] M. Boström, S. Lidin, J. Alloys Compd. 376 (2004) 49.
[5] A. Tengå, S. Lidin, J.-P. Belieres, N. Newman, Y. Wu, U. Häussermann, J. Am. Chem. Soc. 130 (2008) 15564.
[6] A.S. Mikhaylushkin, J. Nylén, U. Häussermann, Chem.-Eur. J. 11 (2005) 4912.
[7] U. Häussermann, A.S. Mikhaylushkin, Dalton Trans. 39 (2010) 1036.
[8] (a) D.M. Rowe (Ed.), CRC Handbook of Thermoelectrics, CRC Press Inc., Florida, 1995;
(b) P.J. Shaver, J. Blair, Phys. Rev. 141 (1966) 649;
(c) T. Caillat, J.-P. Fleurial, A. Borshchevsky, J. Phys. Chem. Solids 58 (1997) 1119;
(d) V.L. Kuznetsov, D.M. Rowe, J. Alloys Compd. 372 (2004) 103;
(e) S.C. Ur, I.H. Kim, P. Nash, J. Mater. Sci. 42 (2007) 2143;
(f) G. Nakamoto, N. Akai, M. Kurisu, J. Alloys Compd. 437 (2007) 151;
(g) B.L. Pedersen, B.B. Iversen, Appl. Phys. Lett. 92 (2008) 161907.
[9] Villars, P.; Calvert, L.D. Pearsons Handbook of Crystallographic Data for Intermetallic Compounds, second ed., ASM International, Materials Park, OH, 1991; Desk Edition, 1997. Prominent representatives are *A*ZnSb (*A*=alkali metal, e.g. LiZnSb (G. Schröder, H.U. Schuster, Z. Naturforsch B 30 (1975) 978) and $AeZn_2Sb_2$ (*Ae*=alkaline earth metal, e.g. $CaZn_2Sb_2$ (A. Mewis, Z. Naturforsch. B 33 (1978) 382). More complex structures and their bonding properties are analyzed in e.g. S. Bobev, J.D. Thompson, J.L. Sarrao, M.M. Olmstead, M. Hope, S.M. Kauzlarich, Inorg. Chem. 43 (2004) 5044; B. Saparov, S.Q. Xia, S. Bobev, Inorg. Chem. 47 (2008) 11237.
[10] A. Tengå, S. Lidin, J.-P. Belieres, N. Newman, Y. Wu, U. Häussermann, Chem.-Eur. J. 15 (2009) 6704.
[11] Y. Wu, S. Lidin, T.L. Groy, N. Newman, U. Häussermann, Inorg. Chem. 48 (2009) 5996.
[12] M. Boström, S. Hovmöller, J. Solid State Chem. 153 (2000) 398.
[13] *CrysAlis*, Software for automated data collection and reduction, Oxford Diffraction, 2006.
[14] G. Oszlanyi, A. Suto, Acta Crystallogr. A 60 (2004) 134.
[15] L. Palatinus, G. Chapuis, J. Appl. Crystallogr. 40 (2007) 786.
[16] V. Petricek, M. Dusek, The Crystallographic Computing System JANA2000, Institute of Physics, Praha, Czech Republic, 2000.
[17] B. Hyde, S. Andersson, in: Inorganic Crystal Structures, John Wiley & Sons, New York, 1989.
[18] G.A. Slack, in: H. Ehrenreich, F. Seitz, D. Turnbull (Eds.), Solid State Physics, vol. 34, Academic Press, New York, 1979, pp. 1–71.
[19] T.M. Tritt (Ed.), Thermal Conductivity: Theory, Properties and Applications, Springer, New York, 2004.